JOURNAL OF PETROLEUM GEOMECHANICS
(JPG)

Sensitivity analysis of effective factors for estimating formation pore pressure using a new method: the LSSVM-PSO algorithm

Meysam Rajabi[1*]; Hamzeh Ghorbani[2]; Saeed Khezerloo-ye Aghdam[3]

1. Department of Mining Engineering, Birjand University of Technology, Birjand, Iran
2. Young Researchers and Elite Club, Ahvaz Branch, Islamic Azad University, Ahvaz, Iran
3. Department of Petroleum Engineering, Amirkabir University of Technology, Tehran, Iran

Received:06 August 2021; Accepted: 10 January 2022
DOI: 10.22107/jpg.2022.298551.1152

Keywords
Pore Pressure
LSSVM-PSO
Feature Selection
Sensitivity Analysis
Hybrid Machine Learning

Abstract

The drilling of hydrocarbon wells is a process in which the drilling team deals with the numerous challenges to access hydrocarbon resources. Understanding the formation pore pressures is important to develop a successful and comprehensive drilling plan that minimize cost and maximize safety. This study evaluates the performance of some empirical models for calculating pore pressure based on petrophysical variables as input parameters. This research also compares the estimated performance of empirical models, efficiency assessment, and limitations caused by the petrophysical. The model presented in this study uses LSSVM-PSO artificial intelligence optimized neural networks as powerful tools in solving complex problems to identify complex relationship between petrophysical input data and the actual measured pore pressure with a modular formation dynamic measurement. Among the proposed network models, LSSVM-PSO, the most accurate model from performance and metric error, is a candidate for sensitivity analysis evaluation on 15 different classes categorized by type and number of petrophysical input data. The best predictive approach among the specified classes belongs to the classes in which gamma-ray log petrophysical data participated as input nodes. This study confirms the effect of gamma log data as an influential factor in estimating the formation pore pressure parameter using artificial intelligence sensitivity analysis to the parameters assigned to the input variables. As can be seen in the results, the amount of RMSE = 1.13895 and R2 = 1.0000 for class -15 and for the total data used, which compared to other classes, these error parameters are much higher. Researchers in future studies can evaluate the results of this study as an efficient mathematical model.

1. Introduction

Determination of pore pressure (pp) is one of the key factors in the drilling, and completion of oil and gas wells (Sayers et al., 2002; Zhang, 2011). The role of this key parameter is important because factors such as "drilling plans, subsurface geomechanical mechanical models, improved oil and gas recovery programs, and reservoir development strategies" depend on the precise determination of formation pore pressure (Addis, 2017; Gutierrez et al., 2006).

Evaluating this parameter (pore pressure) and mentioned cases can lower risks and minimize drilling time and costs (Zhang and Yin, 2017). During the geological process, the sedimentary layers are stacked in layers over a very long time (over millions of years) and gradually compress the accumulation of heavy sedimentary loads on the buried formations. In compacted, impermeable layers enclosed in porous areas, pressurized structural fluids prevent potential reservoirs from escaping (Shi and Wang, 1986). Hydrostatic pressure gradually builds up in sedimentary formations with burial depths under the influence of a functional relationship with overpressure. (Polito et al.,

* Department of Mining Engineering, Birjand University of Technology, Birjand, Iran m.rajabi@birjandut.ac.ir

2008).
Factors that significantly reduce drilling hazards include: "Availability of subsurface pore pressure maps, identification of areas under abnormal pressure" (Rehm et al., 2013). Therefore, the drilling program presented with the knowledge of determining the pore pressure makes these drilling programs more reliable (Osborne and Swarbrick, 1997).
One of the oldest methods used to calculate pore pressure was developed by Eaton in 1948. This method is expressed as Equation (1):

$$S = \sigma + P_P \quad (1)$$

Where:
S = overburden pressure;
σ = matrix stress; and,
P_P = pore pressure.

Eaton (1975) presented an experimental equation for predicting pore pressure based on resistivity log as shown in Equation (2):

$$P_p = \delta_v - (\delta_v - P_{hyd})\left(\frac{R_{log}}{R_n}\right)^n \quad (2)$$

Where:
Pp = the pore pressure;
δ_v = the total vertical stress;
P_{hyd} = the normal or hydrostatic pressure;
R_{log} is the observed resistivity log value;
R_n = the resistivity log associated with a normal pore pressure profile; and,
n = an empirical constant, for which a value of 1.2 is commonly used (Yoshida et al., 1996).
Eaton's empirical formula for predicting pore pressure from sonic well log transit time values is expressed as in Equation (3).

$$P_p = \delta_v - (\delta_v - P_{hyd})\left(\frac{\Delta T_n}{\Delta T_{log}}\right)^n \quad (3)$$

Where:
P_p = the pore pressure;
δ_v = the total vertical stress;
P_{hyd} = the normal or hydrostatic pressure;
ΔT_{log} = the sonic log transit time value;
ΔT_n = the sonic log value when pore pressure is normal;
n = an empirical constant, for which a value of 3.0 is commonly used (Yoshida et al., 1996).
Bowers constructed a model to predict pore pressure using effective stress. The most prominent objective of this work was to determine the effective stresses to predict the pore pressure. This approach used compaction imbalance and expansion of fluids as the most effective mechanisms affecting overpressure generation. (Bowers, 1995).
Mustafa et al. (2012) in 2012 based on Radial Basis Function Neural Network (RBFNN) modelling to predict soil pore-water pressure responses to rainfall, is used. After examinations, the results show that RBFNN is suitable for mapping pores' nonlinear and complex behavior (Mustafa et al., 2012).
Atashbari et al. (2012) calculated effective stress via bulk density data driven from well-log for carbonate reservoirs exist in south west of Iran. Variation in pore pressure while compaction is related to the variation in the porosity. Porosity is also a function of bulk density, which increases in compaction process. Progress in compaction phenomenon results in the reduction of pore volume, which raises the pressure of the fluid present in the porous media. Eq. (4) calculates the pore pressure using the compressibility of rock and pore (Atashbari and Tingay, 2012).

$$P_p = \left(\frac{(1-\emptyset)C_b\sigma_{eff.}}{(1-\emptyset)C_b - \emptyset C_p}\right)^{\gamma} \quad (4)$$

Where:
P_p = pore pressure;
ø = fractional porosity;
C_b = bulk compressibility in psi^{-1};
C_p = pore compressibility in psi^{-1};
σ_{eff} = vertical effective stress in psi; and, γ is an empirical constant, ranging from 0.9 to 1.0.

Keshavarzi and Jahanbakhshi (2013) conducted their studies on an oil field very close to Iran. The Arabian plate contains two oil reservoirs namely Asmari (Oligo-Miocene) and Bangestan (Cretaceous) which are based on a backpropagation algorithm and a generalized regression neural network. This approach predicts pore pressure gradient in the Asmari reservoir, which is comparable to Eaton's method. The study ultimately leads to the conclusion that the back-propagation algorithm and a generalized model regression neural network has higher accuracy than Eaton model (Keshavarzi and Jahanbakhshi, 2013).

Azadpour et al. (2015) proposed a model predicting pore pressure based on empirical approaches in a gas field located in south of Iran (Azadpour et al., 2015): Eaton (Eq. (2)) (Eaton, 1975), Bowers (velocity-based model) (Bowers, 1995) and the compressibility Atashbari and Tingay methods (Atashbari and Tingay, 2012) findings disclosed that the Eaton approach predicts the pore pressure more accurately than other approaches. Therefore, they constructed a model consist of three-dimensional pore pressure. The predicted values for pore pressure using that 3D model were in good agreement with measured ones via a wireline-based modular dynamic tester. Compaction to address the challenge of disequilibrium applies Eq. (5) to Eq. (7) to resolve unloading conditions.

$$\mathrm{V} = V_0 + A\sigma^B \tag{5}$$

$$\mathrm{V} = V_0 + A\left[\sigma_{max}\left(\frac{\sigma}{\sigma_{max}}\right)^{\left(\frac{1}{U}\right)}\right]^B \tag{6}$$

$$\sigma_{max} = \left(\frac{V_{max} - 1500}{A}\right)^{\frac{1}{B}} \tag{7}$$

Where:

V = velocity;

V_0 = the surface velocity (normally 1500 m/sec);

σ = the vertical stress; A and B are obtained from calibrating regional offset velocity versus effective stress data;

U = the unloading parameter;

V_{max} and σ_{max} = velocity and effective stress, respectively, at the onset of unloading.

Ahmed et al. (2019) developed their study based on an onshore well drilled directionally with two different hole sizes of 8 3/8 and 5 7/8. They used the neural network (ANN) based on different trails with different variable inputs, the best and most optimal inputs are selected and identified. In this study, drilling parameters such as weight on bit (WOB), rotational speed (RPM), rate of penetration (ROP), Mud weight (MW), bulk density (RHOB), porosity (φ) and compression time (DT) were also investigated. The results showed that the composition of drilling parameters is very important as data entry into the system to predict high-resolution pores pressure. The new experimental correlation was developed using the Optimized ANN method to estimate pore pressure with high accuracy (0.998 and average correlation coefficient Absolute percentage error 0.17%) (Ahmed et al., 2019a).

In another study in 2019, Ahmed et al. (2019) was conducted their study on a batch drilled branch of offshore petrophysical data using the support vector machine (SVM) algorithm. The wide lithological facies of different formations including five interbedded shales and sandstones at the bottom in a layer of carbonate at the top. They predict pore and fracture pressure with a determination coefficient (R2) of more than 0.995 (Ahmed et al., 2019b).

This research efforts to propose a high-quality intelligence model to predict formation pore pressure. This approach optimizes mathematical models by following the major stages and important goals and introduce the petrophysical gamma-ray dataset as an effective novel input to create more accurate performance on formation pore pressure prediction. the study conducts a

sensitivity analysis on each input variable on output variable to find a good combination for best accuracy.

The LSSVM model is widely implemented by various researchers. However, due to the difficulty in identifying its parameters and its poor robustness and low prediction accuracy, researchers have proposed many methods to optimize and improve the LSSVM model. An intelligent optimization algorithm called Particle Swarm Optimization (PSO) is one of these methods. The PSO-LSSVM model has received a lot of attention due to its fast convergence speed, global optimization capability and high prediction accuracy, especially the penalty coefficient and the core parameters of the LSSVM intelligent optimization model.

This article's main purpose is to use a new sensitivity analysis technique and find a new way to combine these parameters and achieve the best performance accuracy. In this paper, a novel LSSVM-PSO combination technique is used. The most prominent novelty of this paper is to implement a new approach to determine sensitivity analysis and the combination of input parameters to determine the best output result. Other novelties used in this paper are the combination of Particle Swarm Optimization (PSO) optimization algorithm with LSSVM algorithm, which causes fast convergence speed, global optimization ability and high prediction accuracy, especially penalty and nuclear parameters. The LSSVM-PSO model increases the speed and performance of this algorithm.

2. Material method

2.1 Flow Diagram

Figure 1 shows the flow diagram for estimating the pore pressure using the effective factors using the LLSVM-PSO algorithm. Based on this, first the data are collected, then the data are divided into two training and testing subset. After determining and sorting the minimum and maximum of each input variable, the input data were classified into 15 different classes. In order to compare different classes, we use metrics (R2 and RMSE) to compare these classes. Finally, by finding the best class, the aim of the study was to find the most effective input variable factors (SGR and CGR), and finally, in order to validate the LSSVM-PSO model, we used information about the two wells #B and #C.

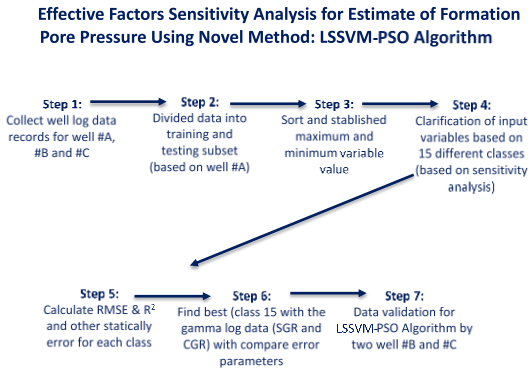

Figure 1. Flow diagram for pore pressure prediction.

2.2 Machine learning algorithm

Today, machine learning algorithms are widely used to construct accurate and applicable predictions of the variables that govern nonlinear and sparse relationships with other influencing variables, as a powerful tool in all oil and gas industry: evaluating production performance (Choubineh et al., 2017; Ghorbani et al., 2017; Ghorbani et al., 2019); CO2 capture (Hassanpouryouzband et al., 2019a; Hassanpouryouzband et al., 2019b; Hassanpouryouzband et al., 2018a, b); reservoir evaluation (Ghorbani et al., 2020), permeability prediction (Yeganeh et al., 2012), fracture modeling (Darabi et al., 2010) and EOR (Jafari et al., 2018).

In this study, three learning algorithms, including Least Squares Support Vector Machine (LSSVM) with an optimizer algorithm, Particle Swarm Optimization (PSO), are employed to develop a hybrid model of predicting PP speedily with high accuracy

2.2.1 Least squares support vector machine (LSSVM) algorithm

LSSVM, developed in 1999 by Suykens and Vandewalle, is an interesting modified form of the conventional Support Vector Machine (SVM) (Suykens and Vandewalle, 1999). SVM is a robust tool in data regression developed by Vapnik et al. (Vapnik, 2013). There are two main differences by which LSSVM can be discriminated from SVM: i) LSSVM uses least square errors in cost function while SVM uses nonnegative errors ii) LSSVM solves complex mathematical problems and problems linearly and solves them easily, while SVM solves mathematical problems and problems in quadratic programming and then solves them. (Yuan et al., 2015). SVM expresses training in terms of quadratic programming (QP) system where a quadratic matrix determines the training point numbers; however, LSSVM expresses training data concerning the linear programming system. LSSVM transforms the QP matrices into linear programming matrices, thereby reducing computational complexity, leading to a considerable reduction in the computation time of the learning model (Kisi and Parmar, 2016). Due to its being more computationally efficient, the LSSVM algorithm has been successfully employed in both regression and classification machine learning for different applications such as time series prediction, fault diagnosis, system modelling, and pattern recognition (Adankon and Cheriet, 2009; Anemangely et al., 2019a; Anemangely et al., 2019b; Lima et al., 2010; Stephen et al., 2014; Tsujinishi and Abe, 2003; Yarveicy et al., 2014; Yu et al., 2008; Zheng et al., 2011).

Considering a defined set of training data (x_i, y_i), $i = 1, 2, 3, \dots, N$, where $x_i \in R$, $y_i \in R$, and N are, respectively, the input data, output data, and the total number of pairs of training data, and x and y are, respectively, dependent and independent variables, LSSVM develops from conventional SVM formulation as expressed in Equation 8:

$$y = w^T \varphi(x) + b \tag{8}$$

Where:

w and b = represent the weight vector and the bias trend, respectively; and

φ(x) = the kernel function, which can be radial, polynomial, basis function (RBF), multiple kernels (

Table).

The cost function, C, for LSSVM is minimized using Equation 9:

$$\begin{aligned} & min\, C(w,e) = \frac{1}{2} w^T w + \frac{1}{2}\gamma \sum_{i=1}^{N} e_i^2 \\ & subject\ to \quad y = w^T \varphi(x_i) + b + e_i \end{aligned} \tag{9}$$

Where:

y = represent the regularized parameter requiring establishing a compromise between smoothness and the minimization of training error. Typically, a Lagrangian algorithm, as formulated in Equation 10, is used to solve this optimization.

$$L(w,b,e,\alpha) = \frac{1}{2}\|w\|^2 + \gamma \sum_{i=1}^{N} e_i^2 - \sum_{i=1}^{N} \alpha_i \{w^T \varphi(x_i) + b + e_i - y_i\} \tag{10}$$

Where:

αi = values that can be either negative or positive are the multipliers of the Lagrange can be determined by taking a differentiate of Equation 12 with w, b, α_i, e_i. The optimality conditions for this problem can be acquired where all four derivatives are set equal to zero as shown in expressions (Equation 11-14)

$$\frac{\partial L}{\partial w} = 0 \rightarrow w = \sum_{i=1}^{N} \alpha_i \varphi(x_i) \quad (11)$$

$$\frac{\partial L}{\partial b} = 0 \rightarrow \sum_{i=1}^{N} \alpha_i = 0 \quad (12)$$

$$\frac{\partial L}{\partial e_i} = 0 \rightarrow \alpha_i = \gamma e_i \ , \quad i = 1,2,\dots,N \quad (13)$$

$$\frac{\partial L}{\partial \alpha_i} = 0 \rightarrow w^T \varphi(x_i) + b + e_i - y = \gamma e_i \quad , \quad i = 1,2,\dots,N \quad (14)$$

Therefore;

$$w = \sum_{i=1}^{N} \alpha_i \varphi(x_i) = \sum_{i=1}^{N} \gamma e_i \varphi(x_i) \quad (15)$$

Weights are linear summations of the Lagrange multipliers applied for dataset training the (x_i). Substituting the results of (15) into (8) will result in Equation 16:

$$y = \sum\nolimits_{i=1}^{N} \alpha_i \varphi(x_i)^T \varphi(x) + b = \sum\nolimits_{i=1}^{N} \alpha_i K(x_i, x) + b \quad (16)$$

Table 1. Kernel functions are commonly applied with the LSSVM algorithm (Kisi and Parmar, 2016).

Linear (lin-kernel)	$\boldsymbol{K(x, x_i) = x_i^T x}$	-
Polynomial (poly-kernel)	$K(x, x_i) = \left(t + \frac{x_i^T x}{c}\right)^d$	t and d are the intercepts and the degree of the polynomial.
Radial basis function (RBF-kernel)	$K(x, x_i) = exp\left(-\frac{\|x - x_i\|^2}{\sigma^2}\right)$	σ^2 is the variance of the Gaussian kernel.
Multi-layer perceptron (MLP-kernel)	$K(x, x_i) = tanh(kx_i^T x + \theta)$	θ and k are bias and scale parameters, respectively.

2.2.2 Particle swarm optimization (PSO) algorithm

The PSO algorithm was developed by American scholars Kennedy and Eberhart in 1995 (Kennedy, 1997; Kennedy and Eberhart, 1995). This algorithm is a stochastic optimization technique originating from analyzing a swarm of birds (Gandomi et al., 2013; Yang and Papa, 2016). In a combination of other algorithms, the PSO algorithm has been widely used to solve many nonlinear problems of the petroleum industry (Atashnezhad et al., 2014). It moves all the individuals of a population ("swarm") around, seeking a potential optimal solution. The PSO's optimal solution is typically described as the minimum squared error (MSE) related to the objective function. At first, each swarm particle is given a defined random position and velocity based on their upper and lower limits. PSO performs several iterations of particles moving around to find the space solution. From one iteration to the next, each particle's position is adjusted using information connected to its best personal position (P_b) and the best global position of the swarm (G_b) related to the objective function. At each iteration, PSO endeavors to minimize the related cost function of objective function. (P_b) is considered as a distinctive feature of PSO algorithm because of it retaining the historical information of

each particle, by which the particle repositioning is effectively performed. For each irritation, particles' velocity, (P_b), and (G_b) are adjusted. The velocity of a particle for next iteration, ($V_i(t+1)$), can be defined by means of the particle's velocity in the previous iteration, together with the distance of the particle from its best specific position, which is likely reached serval iteration before, and the current best global position of the particles' population (Equation 17). The position of the particle for the next iteration ($x_i(t+1)$) is adjusted by adding the calculated velocity to the current position of the particle (Equation 18).

$$V_i(t+1) = wV_i(t) + c_1 r_1\big(Pb_i(t) - x_i(t)\big) + c_2 r_2(G_b(t) - x_i(t)) \quad (17)$$

$$x_i(t+1) = x_i(t) + V_i(t+1) \quad (18)$$

Where:

i = series making up of n elements;

n = represents the number of particles forming the swarm;

w = refers to inertia, a coefficient (weight) moderating the calculation of velocity for each the swarm's particle, which takes values usually ranging from 0 to 1 (Pedersen and Chipperfield, 2010);

$r_1\ and\ r_2$ = refer to two random vectors, $c_1\ and\ c_2$ are two nonnegative cognitive and social acceleration coefficients, respectively (Coello et al., 2007).

The c_1 represents the learning adjustment for individual particles and c_2 represents the learning adjustment for the population (whole swarm).

The best method for establishing the values for weight, cognitive, and social acceleration coefficients is conducting trial and error tests on each given data set to be evaluated.

According to the new location of each particle obtained using Equation 20, the cost (objective) function for each particle is recalculated for iteration $(t+1)$. The particle's best (P_b) remains unchanged for iteration $(t+1)$ If the current cost value of the particle is greater or equal to its previous best (P_b), whereas the position of the particle is updated for $(t+1)$ if its current cost value is less than that of its previous one. The best (G_b) for the population is also updated according to each particle's new location and the previous population's (G_b). The algorithm's progress toward the optimal solution is monitored by retaining each iteration's best (Gb) locations.

2.2.3 Hybrid PSO-LSSVEM machine learning model

This approach is successfully applied in many fields. The radial- basis- kernel function (RBF, see table 1) is employed to guide the LSSVM-PSO model used for predicting PP in the dataset this work analyses. For tuning the hyperparameters influencing the LSSVM prediction performance, a PSO optimizer is used, which determines the optimum values for the regularization parameter, γ, and Gaussian RBF kernel's variance σ^2. Table 1 shows the optimal values for the γ and σ^2 determined for the hybrid LSSVM model employed in this study.

Table 2. Optimal values for Gaussian RBF kernel's variance regularization parameter for developed hybrid LSSVM-PSO used for PP prediction.

Parameters	Values
Regularization parameter (y)	0.6814
The variance of Gaussian RBF kernel ($\boldsymbol{\sigma^2}$)	2.2065

3. Data collection

The information collected in this research is related to the data of three wells #A, #B and #C from one of the fields in the southwest of Iran, which is used for sensitivity analysis as well as the construction of an artificial intelligence network using information related to well #A between depths of 3665.2

m and 4005.2 m at a data recording interval of 0.2m. Information on #B between depths of 3321.6 m and 3523.4 m at a data recording interval of 0.2m and #C between depths of 3547.0 m and 3727.0 m at a data recording interval of 0.2m wells has been used to validate.

Use the Eaton model to determine the pore pressure, then use the Repeat Formation Tester (RFT) Downhole Direct Pressure Measurements to measure the pore pressure at depths of 3668m, 3766m, 3834m and 3901m, then verify the data using these pressures.

1700 data sets are related to well #A, of which 85% are for training and 15% for testing. The data used in this study are petrophysical data derived from common tools (Atashnezhad et al., 2014; Darling, 2005; Ghasemi and Bayuk, 2020; Liu, 2017). Effective overburden pressure (δ_{eff}), pore compressibility (Cp), corrected gamma rays (CGR) adjusted for uranium recorded as part of the set of gamma-ray spectral curves (SGR; with data for the potassium (POTA), thorium (THOR) and uranium (URAN)), photoelectric absorption factor (PEF), formation bulk density (RHOB), sonic compression transition time (DT), neutron porosity (NPHI) and Deep Resistivity (ILD) logs. This data has been used as input variable data for artificial intelligence. For validation of the algorithm, we used well #A and well #B. Table 3 shows statistical details obtained by SPSS software for total data for well #A, well #B, and #C.

Table 3. Data record statistical characterization of the variables in the complete well-log dataset for well #A, #B and #C.

Well No.	Parameters	δ_{eff}	Cp	CGR	SGR	PEF	RHOB	DT	NPHI	ILD	Pore Pressure
-	Units	Psi	1/Psi	API	API	Barns /cm^3	g/cm^3	µs/ft	(%)	ohm-m	Psi
Well #A	Mean	4533.7	3.71E-06	24.2	43.7	4.4	2.96	72.1	15.3	1174.0	4744.1
	Std. Deviation	335.2	2.54E-06	22.6	23.3	1.3	0.59	16.5	7.0	4282.8	351.3
	Variance	91671.7	2.41E-06	410.8	440.4	1.3	0.44	89.8	33.0	18234893.7	116148.3
	Minimum	2179.3	3.47E-06	3.5	14.6	2.3	1.61	58.5	2.8	11.8	4102.6
	Maximum	5113.3	4.48E-06	123.8	146.0	6.7	3.28	124.6	48.1	20011.4	5385.8
Well #B	Mean	4892.8	3.82E-06	54.5	38.5	5.2	3.08	79.5	12.9	825.4	4887.4
	Std. Deviation	277.4	2.67E-06	31.7	18.4	2.2	0.53	16.0	8.4	3458.3	278.8
	Variance	59984.8	2.41E-06	858.4	256.4	3.7	0.43	80.5	49.8	11871386.2	72005.0
	Minimum	4403.6	3.51E-06	7.5	8.4	3.0	2.76	49.3	2.4	11.8	4484.4
	Maximum	5467.4	4.66E-06	112.7	80.7	9.1	3.39	96.7	36.1	20011.4	5553.4
Well #C	Mean	4637.7	3.80E-06	62.4	39.9	15.3	2.93	67.4	13.4	1209.6	4870.4
	Std. Deviation	358.0	4.21E-06	12.0	15.4	3.2	0.54	17.0	7.2	4421.3	178.5
	Variance	105951.3	2.41E-06	94.2	171.2	8.4	0.43	99.2	35.5	19431016.1	28245.7
	Minimum	3812.2	-3.78E-05	50.8	16.0	4.7	2.12	55.8	1.4	11.9	4508.4
	Maximum	5224.8	4.31E-05	102.7	91.9	17.9	2.77	107.7	35.8	20011.4	5438.4

4. Result and disscusion

The comparison is based on computational errors. These measures are percentage deviation (PDi), average relative error

(ARE), average absolute relative error (AARE), standard deviation (SD), mean square error (MSE), root mean square error (RMSE), and coefficient of determination (R^2). The computation formulas for these statistical measures are expressed in Equation (19) to Equation (25).

$$PD_i = \frac{\xi_{(Measured)} - \xi_{(Predicted)}}{\xi_{(Measured)}} x\ 100 \quad (19)$$

$$ARE = \frac{\sum_{i=1}^{n} PD_i}{n} \quad (20)$$

$$AARE = \frac{\sum_{i=1}^{n} |PD_i|}{n} \quad (21)$$

$$SD = \sqrt{\frac{\sum_{i=1}^{n} (D_i - Dimean)^2}{n-1}} \quad (22)$$

$$Dimean = \frac{1}{n}\sum_{i=1}^{n}\left(\xi_{Measured_i} - \xi_{Predicted_i}\right)$$

$$MSE = \frac{1}{n}\sum_{i=1}^{n}\left(\xi_{Measured_i} - \xi_{Predicted_i}\right)^2 \quad (23)$$

$$RMSE = \sqrt{MSE} \quad (24)$$

$$R^2 = 1 - \frac{\sum_{i=1}^{N} (\xi_{Predicted_i} - \xi_{Measured_i})^2}{\sum_{i=1}^{N} (\xi_{Predicted_i} - \frac{\sum_{I=1}^{n} \xi_{Measured_i}}{n})^2} \quad (25)$$

The main purpose of this method is to select and determine the optimal combination of the nine input variables (characteristics) listed in Table 4, which helps to minimize the RMSE pore pressure values. The input variables were divided into 15 classes, and Table 5 of these classifications and input variables is arranged separately.

Table 4. Determination of input variables and symbol code.

Input Variable	Symbol Code
PEF	M1
RHOB	M2
DT	M3
NPHI	M4
ILD	M5
δ_{eff}	M6
Cp	M7
CGR	M8
SGR	M9

Table 5. Classification of pore pressure predicted for input variable.

Models	Input variables
Class-1	M2 and M7
Class-2	M6 and M2
Class-3	M3 and M6
Class-4	M2, M3 and M6
Class-5	M7, M6, M2 and M3
Class-6	M5 and M6
Class-7	M6, M7, M2 and M5
Class-8	M3, M6 and M5
Class-9	M2, M3, M5, M6 and M7
Class-10	M4, M7 and M6
Class-11	M7, M2, M6 and M4
Class-12	M5, M3, M2, M7, M4 and M6
Class-13	M9, M7, M6 and M8
Class-14	M1, M2, M8, M9, M6 and M7
Class-15	M6, M7, M8, M9, M1, M2, M3, M4 and M5

Of the 1700 data records in the dataset for well #A, for each model evaluation, 1445 (~85%) data records, spread across the full

pore pressure value range, are allocated to the training subset. The remaining 255 data, also records spread across the full pore pressure value range, are allocated to the testing subset. Each feature selection class is trained and tested with such subsets. Pore pressure prediction error analysis is reported for the Class 1 to Class 15 evaluated for the same training subset (Table 6) and same testing subset (Table 7) and with the optimum solution derived for each class applied to the full dataset (1700 data records, Table 8). The effective overburden pressure (δ_{eff}), as an inherent influencing factor of pore pressure in subsurface formations, is included in the feature selection of all classes except Class 1.
The Classes that include just two input variables (Classes 1,2, 3 and 6) in their feature selection provide the least accurate pore pressure predictions in well #A. Class 6 (δ_{eff} and ILD) provide the worst pore pressure prediction accuracy followed by Class 1 (Cp and RHOB), suggesting that these variables are not combining in a meaningful way to predict pore pressure.
Therefore, what can be deduced from these classes in Tables 6 to 8 is that the combination of parameters such as δ_{eff} and ILD for predicting pore pressure have lower operating accuracy. So if the input variables contain only these two input variables Pore pressure is not well predicted.
The Classes that include just three input variables (Classes 4, 8 and 10) in their feature selection provide the least accurate pore pressure predictions in well #A. Class 10 (δ_{eff}, NPHI and Cp) provide the worst pore pressure prediction accuracy followed by Class 4 (δ_{eff}, RHOB and DT), suggesting that these variables are not combining in a meaningful way to predict pore pressure.
Therefore, what results from these classes in Tables 6 to 8 is that the combination of parameters such as δ_{eff}, NPHI and Cp to predict the pore pressure have lower performance accuracy. So if the input variables contain only these two variables Inlet pore pressure is not well predicted.
The Classes that include just four and five input variables (Classes 5, 7, 9, 11 and 13) in their feature selection provide the least accurate pore pressure predictions in well #A. Class 11 (δ_{eff}, RHOB, NPHI and Cp) provide the worst pore pressure prediction accuracy followed by Class 13 (δ_{eff}, Cp, CGR and SGR), suggesting that these variables are not combining in a meaningful way to predict pore pressure.
Therefore, what can be deduced from these classes in Tables 6 to 8 is that the combination of parameters such as δ_{eff}, RHOB, NPHI and Cp to predict the pore pressure have lower performance accuracy. So, if the input variables only include this If the input variables are two, the pore pressure is not well predicted.
Class 14, including just six variables (δ_{eff}, Cp, CGR, SGR, PEF, RHOB) in its feature selection, achieve prediction accuracy only slightly lower than Class 15. This suggests that variables DT, NPHI and ILD only improve the prediction performance of Class 14 by a small amount when included in the feature selection of Class 15. On the other hand, the inclusion of the PEF variable in class 14 and class 15 seems to be a critical factor to improve their pore pressure prediction performance compared to class 13, which offers the third-best prediction performance when starting with only four input variables (δ_{eff}, Cp, CGR, SGR).
Class 15 feature selection with all nine input variables included (δ_{eff}, Cp, CGR, SGR, PEF, RHOB, DT, NPHI and ILD) achieves the most accurate pore pressure prediction of all the combinations of input variables tested, for the subsets and full dataset (Tables 6 to 8). The Class 15 feature selection achieves impressive pore pressure prediction accuracy (9 input variables applied to all 1700 data records: RMSE= 1.139 and R^2 = 1) as do Class 14 (6 input variables applied to all 1700 data records: RMSE= 1.663 and R^2 = 1) and Class 13 (4 input variables applied to all 1700 data records: RMSE= 3.634 and R^2 = 0.999). These are the only classes to include gamma-

ray (both CGR and SGR).
According to the results obtained in this class, we find that gamma-ray has a significant effect in predicting pore pressure.

Table 6. Pore pressure prediction accuracy achieved by the LSSVM-PSO algorithm applied to the complete dataset characterized for train data.

Models	ARE%	AARE%	SD	MSE	RMSE	R^2
Class-1	-0.08678	0.91898	67.5146	4571.85770	67.6155	0.9680
Class-2	-0.08535	0.79969	60.2248	3613.97782	60.1163	0.9750
Class-3	-0.06907	0.61416	48.6487	2389.72060	48.8847	0.9826
Class-4	-0.00525	0.09859	7.94739	63.16094	7.94739	0.9995
Class-5	-0.00014	0.06480	5.57484	31.61708	5.62291	0.9998
Class-6	-0.32708	2.49366	173.698	30267.7125	173.976	0.7459
Class-7	-0.00031	0.08328	6.45786	45.65087	6.75654	0.9997
Class-8	-0.04270	0.40686	33.1248	1093.75318	33.0719	0.9925
Class-9	-0.00049	0.06022	5.65545	27.71738	5.26473	0.9998
Class-10	-0.05543	0.51393	39.0154	1552.84982	39.4062	0.9898
Class-11	0.00195	0.09382	7.15455	51.00569	7.14183	0.9996
Class-12	-0.00194	0.05861	4.83584	23.25176	4.82201	0.9998
Class-13	-0.00449	0.04862	3.87875	15.44766	3.93035	0.9999
Class-14	-0.00230	0.02161	1.65482	3.23865	1.79963	1.0000
Class-15	-0.00153	0.01423	1.22154	1.51737	1.23181	1.0000

Table 7. Pore pressure prediction accuracy achieved by the LSSVM-PSO algorithm applied to the complete dataset characterized for test data.

Models	ARE%	AARE%	SD	MSE	RMSE	R^2
Class-1	0.13541	0.98455	64.9678	4220.57467	64.96595	0.9789
Class-2	0.22875	0.76642	63.4843	4031.01159	63.49025	0.9773
Class-3	0.19342	0.59792	47.1257	2219.55424	47.11215	0.9865
Class-4	0.00389	0.07591	5.86789	34.47420	5.87147	0.9998
Class-5	0.00803	0.03184	2.89478	8.33326	2.88674	0.9999
Class-6	0.56402	2.37889	159.836	25550.32266	159.84468	0.8282
Class-7	0.00790	0.05178	4.41478	19.89562	4.46045	0.9999
Class-8	0.12910	0.37792	31.8234	1013.45013	31.83473	0.9940
Class-9	0.00586	0.02875	2.36478	5.54878	2.35558	1.0000
Class-10	0.15649	0.49657	45.3147	2036.97747	45.13289	0.9878
Class-11	0.00721	0.06788	5.62478	31.76059	5.63565	0.9998
Class-12	0.00990	0.03288	2.87645	8.67099	2.94466	0.9999
Class-13	0.00447	0.02599	2.71154	7.43141	2.72606	0.9999
Class-14	0.00155	0.00974	0.89457	0.80454	0.89696	1.0000
Class-15	-0.00074	0.00436	0.35586	0.19356	0.43995	1.0000

Figures 2 and 3 display predicted pore pressure values versus measured ones evaluated by Classes 1 to 15 which applied to all 1700 data records (Table 8) for well #A. Classes 12 to 15 (Figure 3) stand out as the most accurate pore pressure prediction models. On the other hand, Classes 6, 1, 2, 3 (Figure 2) and 10 (Figure 3) standouts, in that order, as the least accurate pore pressure prediction models. The lowest pore pressure prediction accuracies actually achieved by the LSSVM-PSO model applied to all 1700 data records were for Class 6 with RMSE= 160.860 and R^2 = 0.759, Class 1 with RMSE= 62.518 and R^2 =0.869, and Class 2 with RMSE= 55.584 and R^2 = 0.975.

One of the factors shown in Figures 2 and 3 is that when the SGR and CGR input variables are added to the input variables, the LSSVM-PSO model built in that class is more resistant to the outlier data. Give. Based on the results in these two figures, it can be

concluded that the two input variables SGR and CGR are two of the most influential input variables for predicting pore pressure. By comparing these two figures (Figures 2 and 3) as well as the results in Tables 6 to 8, it can be concluded that classes 12 to 15 have the highest performance accuracy.

The highest pore pressure prediction accuracies actually achieved by the LSSVM-PSO model applied to all 1700 data records were for Class 12 with RMSE= 4.45850 and R^2 = 0.9999, Class 12 with RMSE= 3.63406 and R^2 = 0.9999, Class 14 with RMSE= 1.66396 and R^2 =1.0000, and Class 15 with RMSE= 1.13895 and R^2 = 1.0000.

Table 8. Pore pressure prediction accuracy achieved by the LSSVM-PSO algorithm applied to the complete dataset characterized for total data.

Models	ARE%	AARE%	SD	MSE	RMSE	R^2
Class-1	-0.07419	0.78565	62.52457	3908.53013	62.51824	0.9699
Class-2	-0.07296	0.68366	55.58364	3089.62836	55.58443	0.9754
Class-3	-0.05905	0.52505	45.18453	2042.99774	45.19953	0.9832
Class-4	-0.00448	0.08429	7.33355	53.99696	7.34826	0.9996
Class-5	-0.00012	0.05540	5.19741	27.02978	5.19902	0.9998
Class-6	-0.27962	2.13186	160.821	25876.19178	160.86078	0.7591
Class-7	-0.00026	0.07120	6.24124	39.02742	6.24719	0.9997
Class-8	-0.03651	0.34783	30.5634	935.06131	30.57877	0.9927
Class-9	-0.00042	0.05148	4.86447	23.69588	4.86784	0.9998
Class-10	-0.04739	0.43937	36.4336	1327.54795	36.43553	0.9895
Class-11	0.00167	0.08021	6.60143	43.60531	6.60343	0.9997
Class-12	-0.00166	0.05011	4.45664	19.87818	4.45850	0.9999
Class-13	-0.00384	0.04156	3.63217	13.20637	3.63406	0.9999
Class-14	-0.00196	0.01847	1.66223	2.76876	1.66396	1.0000
Class-15	-0.00130	0.01216	1.13173	1.29721	1.13895	1.0000

5. Data validation for LSSVM-PSO algorithm

Based on the results of the existing LSSVM-PSO algorithm used to predict the pore pressure used for well #A, it was determined that class 15 (not the input variable) has the best result for this algorithm. However, to validate the LSSVM-PSO algorithm for well #B and #C for this class, the results are presented in Table 9. Based on the results presented in this table, it is determined that this algorithm can be used for other wells with other fields.

Table 9. Validation of LSSVM-PSO algorithm based on well #A to pore pressure prediction for complete datasets of well #B and #C.

Models	ARE%	AARE%	SD	MSE	RMSE	R^2
Well #B	-0.00103	0.0245	1.12454	1.21346	1.12489	1.0000
Well #C	-0.00114	0.0214	1.16478	1.27448	1.12677	0.9999

Figures 4 and 5 show the actual and predicted pore pressure values for validating the LSSVM-PSO algorithm for all well #B and #C data sets. According to these figures, it is clear that the performance accuracy of the LSSVM-PSO algorithm can be used to predict pore pressure for other wells and other fields and has good performance.

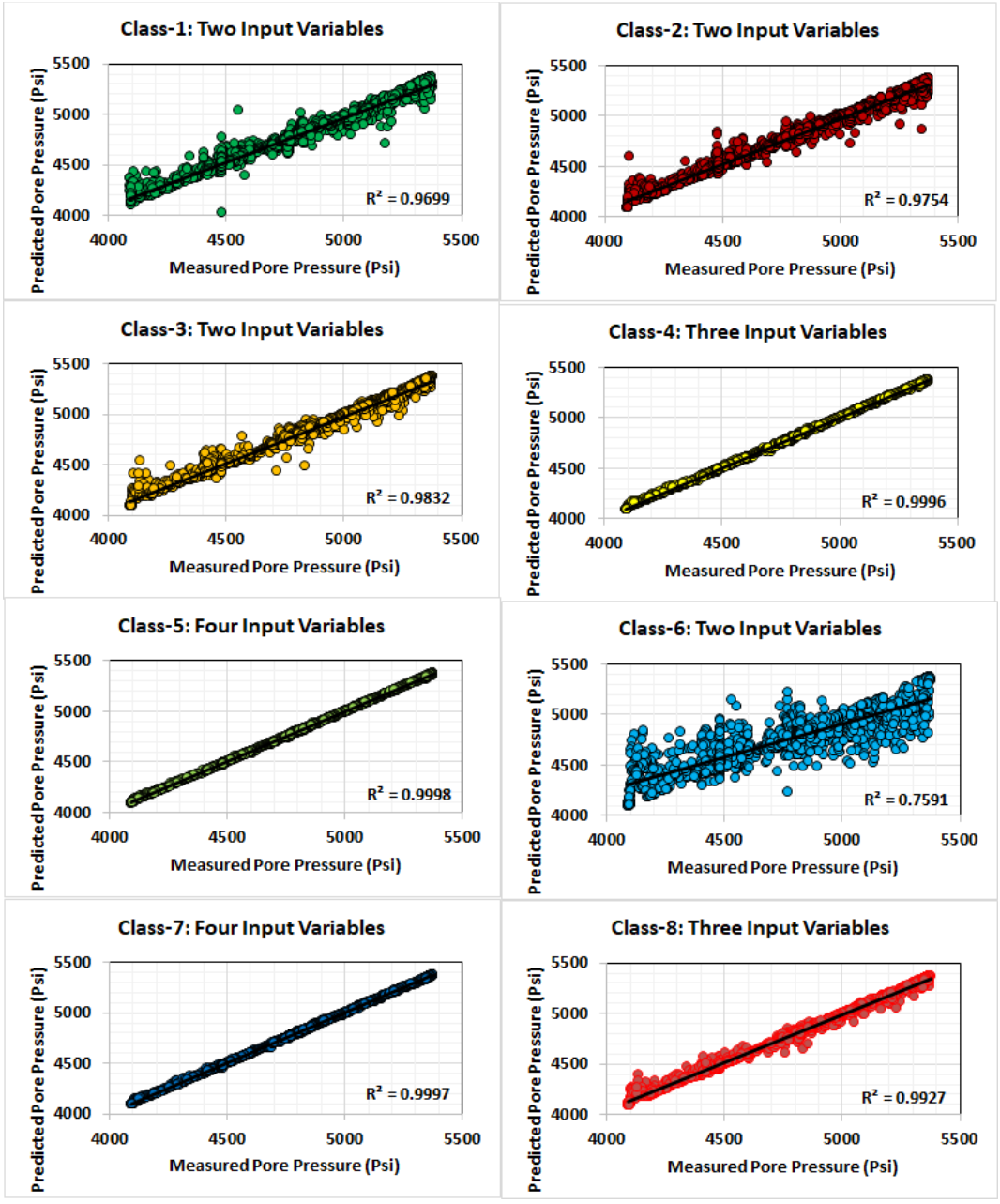

Figure 2. Predicted versus measured pore pressure comparisons for the LSSVM-PSO machine-learning-optimizer model applied to the complete well #A dataset of 1700 data records (Table 8) with Class 1 to Class 8 feature selections.

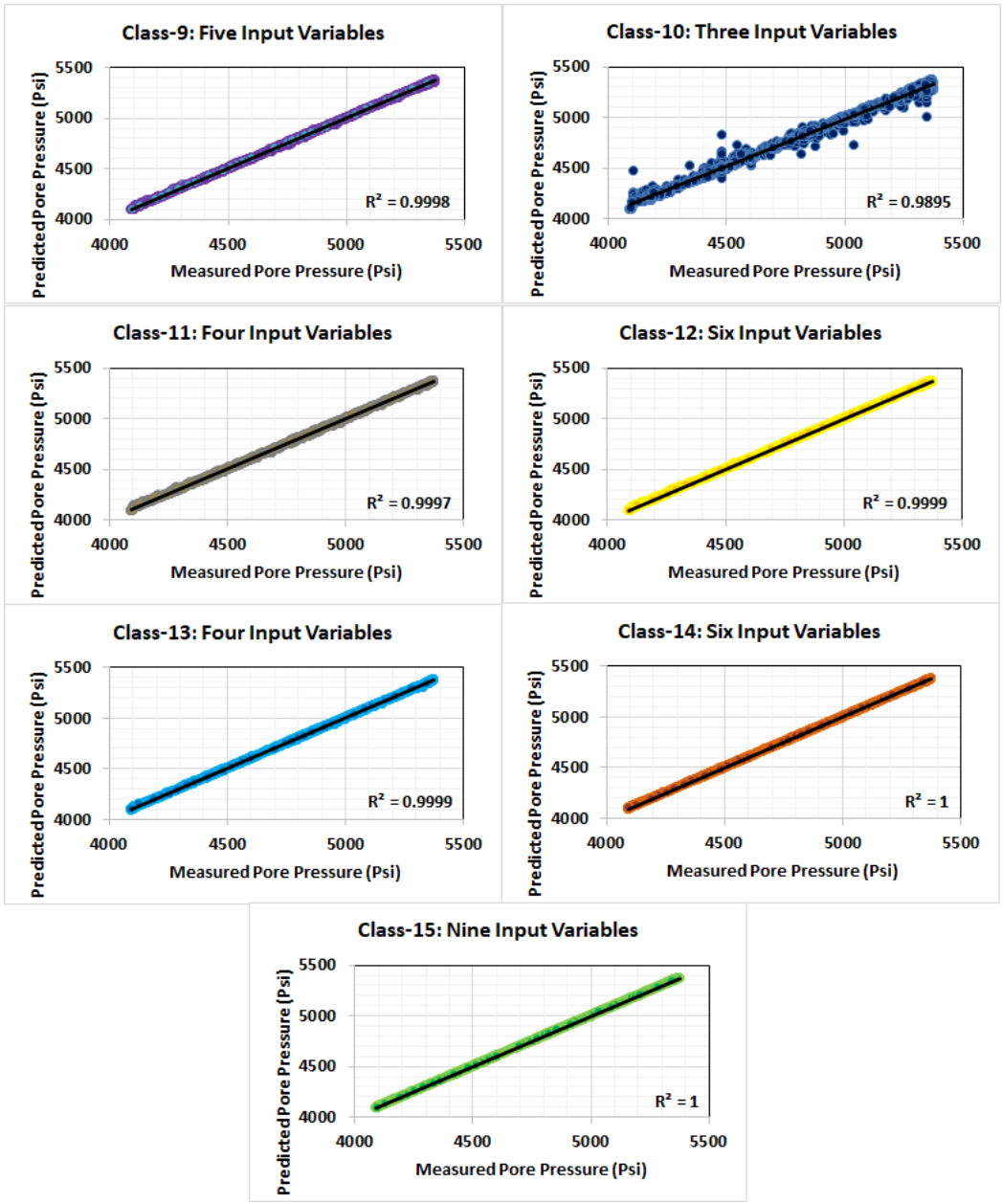

Figure 3. Predicted versus measured pore pressure comparisons for the LSSVM-PSO machine-learning-optimizer model applied to the complete well #A dataset of 1700 data records (Table 8) with Class 9 to Class 15 feature selections.

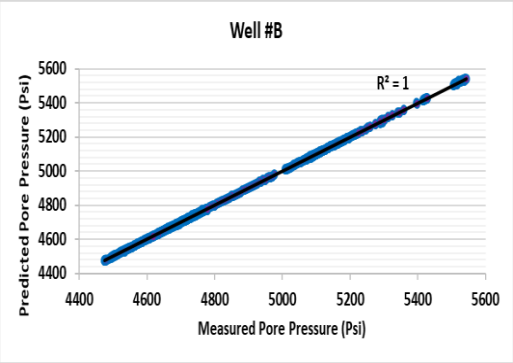

Figure 4. Cross plot of predicted versus measured pore pressure values compared for the LSSVM-PSO model (trained with data from well #A) for information about well #B.

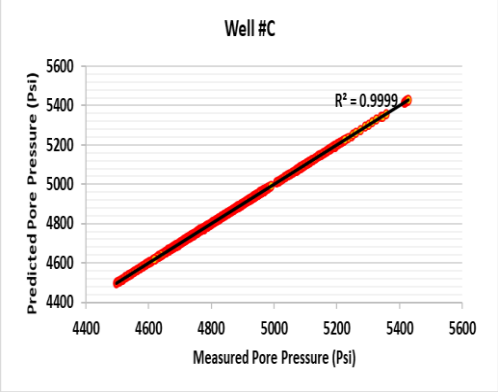

Figure 5. Cross plot of predicted versus measured pore pressure values compared for the LSSVM-PSO model (trained with data from well #A) for information about well #C.

6. Conclusion

This paper predicts the formation pore pressure for three wells, #A, #B, and #C, present in the southwestern oil fields using one of the hybrid machine-learning-optimizer models, LSSVM-PSO.

This algorithm (LSSVM-PSO) can produce accurate and robust classification results based on theoretical foundations, even if the non-uniform and nonlinear input data are separable and help to evaluate the relevant information more easily. Although LSSVM-PSO does not provide a parameter score function, its local linear approximation can be important for understanding the mechanisms that link different financial ratios to a company's final score. For these reasons, LSSVM-PSOs are considered a useful tool to complement the information obtained from classical linear classification techniques effectively.

To commence, we performed a sensitivity study by combining input variables (15 classes) suitable to obtain an output with high-performance accuracy. The sensitivity analysis of the artificial intelligence was performed by the best-proven model of LSSVM-PSO for 15 different classes consisted of types and numbers of petrophysical data inputs. The best predictive performance among the specified classes belongs to the classes in which gamma-ray log petrophysical data participated as input nodes. This study confirms the effect of gamma log data as a strong factor in estimating the hole pressure parameter using artificial intelligence sensitivity analysis to the parameters assigned to the input nodes. Researchers in future studies can evaluate the results of this study to have an efficient mathematical model. Feature selection sensitivity analysis establishes that the LSSVM-PSO model incorporating all nine input variables provides the most accurate pore pressure predictions (RMSE = 1.139 psi for a pore pressure range encountered of 1283 psi). It also achieves similar prediction accuracy when tested with data from two other wells drilled in the field. The results further indicate that the LSSVM-PSO models involving gamma-ray and photo-electric absorption factor (PEF) log-input variables perform better in pore pressure prediction than those that do not.

Results obtained for wells #B and #C illustrates that the prediction accuracy of this algorithm is acceptable in this field. Results from performance accuracy for wells #B and #C resulted in RMSE = 1.1248 psi and RMSE = 1.1267 psi, respectively, which indicates the high performance accuracy of this model.

Acknowledgement

The authors are grateful to Ms Fatemeh Kalaei for his technical support and efforts in collecting the data needed for this study

References

Adankon, M.M., Cheriet, M., 2009. Model selection for the LS-SVM. Application to handwriting recognition. Pattern Recognition 42, 3264-3270. doi: https://doi.org/10.1016/j.patcog.2008.10.023.

Addis, M.A., 2017. The geology of geomechanics: petroleum geomechanical engineering in field development planning. Geological Society, London, Special Publications 458, 7-29. doi: https://doi.org/10.1144/SP458.7.

Ahmed, A., Elkatatny, S., Ali, A., Mahmoud, M., Abdulraheem, A., 2019a. New Model for Pore Pressure Prediction While Drilling Using Artificial Neural Networks. Arabian Journal for Science and Engineering 44, 6079-6088. doi: https://doi.org/10.2118/192318-MS.

Ahmed, S., Mahmoud, A.A., Elkatatny, S., Mahmoud, M., Abdulraheem, A., 2019b. Prediction of Pore and Fracture Pressures Using Support Vector Machine, International Petroleum Technology Conference. International Petroleum Technology Conference. doi: https://doi.org/10.2523/IPTC-19523-MS.

Anemangely, M., Ramezanzadeh, A., Amiri, H., Hoseinpour, S.-A., 2019a. Machine learning technique for the prediction of shear wave velocity using petrophysical logs. Journal of Petroleum Science and Engineering 174, 306-327. doi: https://doi.org/10.1016/j.petrol.2018.11.032.

Anemangely, M., Ramezanzadeh, A., Behboud, M.M٢٠١٩ ,.b. Geomechanical parameter estimation from mechanical specific energy using artificial intelligence. Journal of Petroleum Science and Engineering 175, 407-429. doi: https://doi.org/10.1016/j.petrol.2018.12.054.

Atashbari, V., Tingay, M., 2012. Pore pressure prediction in carbonate reservoirs. OnePetro. doi: https://doi.org/10.2118/150835-MS.

Atashnezhad, A., Wood, D.A., Fereidounpour, A., Khosravanian, R., 2014. Designing and optimizing deviated wellbore trajectories using novel particle swarm algorithms. Journal of Natural Gas Science and Engineering 21, 1184-1204. doi: https://doi.org/10.1016/j.jngse.2014.05.029.

Azadpour, M., Manaman, N.S., Kadkhodaie-Ilkhchi, A., Sedghipour, M.-R., 2015. Pore pressure prediction and modeling using well-logging data in one of the gas fields in south of Iran. Journal of Petroleum Science and Engineering 128, 15-23. doi: https://doi.org/10.1016/j.petrol.2015.02.022.

Bowers, G.L., 1995. Pore pressure estimation from velocity data: Accounting for overpressure mechanisms besides undercompaction. SPE Drilling & Completion 10, 89-95. doi: https://doi.org/10.2118/27488-PA.

Choubineh, A., Ghorbani, H., Wood, D.A., Moosavi, S.R., Khalafi, E., Sadatshojaei, E., 2017. Improved predictions of wellhead choke liquid critical-flow rates: modelling based on hybrid neural network training learning based optimization. Fuel 207, 547-560. doi: https://doi.org/10.1016/j.fuel.2017.06.131.

Coello, C.A.C., Lamont, G.B., Van Veldhuizen, D.A., 2007. Evolutionary algorithms for solving multi-objective problems. Springer.

Darabi, H., Kavousi, A., Moraveji, M., Masihi, M., 2010. 3D fracture modeling in Parsi oil field using artificial intelligence tools. Journal of Petroleum Science and Engineering 71, 67-76. doi: https://doi.org/10.1016/j.petrol.2010.01.004.

Darling, T., 2005. Well logging and formation evaluation. Elsevier.

Eaton, B.A., 1975. The equation for geopressure prediction from well logs. OnePetro. doi: https://doi.org/10.2118/5544-MS.

Gandomi, A.H., Yang, X.-S., Talatahari, S., Alavi, A.H., 2013. Metaheuristic applications in structures and infrastructures. Newnes.

Ghasemi, M., Bayuk, I., 2020. Bounds for Pore Space Parameters of Petroelastic Models of Carbonate Rocks. IZVESTIYA, PHYSICS OF THE SOLID EARTH 56. doi:

Ghorbani, H., Moghadasi, J., Wood, D.A., 2017. Prediction of gas flow rates from gas condensate reservoirs through wellhead chokes using a firefly optimization algorithm. Journal of Natural Gas Science and Engineering 45, 256-271. doi :

Ghorbani, H., Wood, D.A., Choubineh, A., Mohamadian, N., Tatar, A., Farhangian, H., Nikooey, A., 2020. Performance comparison of bubble point pressure from oil PVT data: Several neurocomputing techniques compared. Experimental and Computational Multiphase Flow 2, 225-246. doi :

Ghorbani, H., Wood, D.A., Moghadasi, J., Choubineh, A., Abdizadeh, P., Mohamadian, N., 2019. Predicting liquid flow-rate performance through wellhead chokes with genetic and solver optimizers: an oil field case study. Journal of Petroleum Exploration and Production Technology 9, 1355-1373 :

Gutierrez, M.A., Braunsdor, N.R., Couzens, B.A., 2006. Calibration and ranking of pore-pressure prediction models. The Leading Edge 25, 1516-1523. doi: https://doi.org/10.1190/1.1500391.

Hassanpouryouzband, A., Yang, J., Okwananke, A., Burgass, R., Tohidi, B., Chuvilin, E., Istomin, V., Bukhanov, B., 2019a. An Experimental Investigation on the Kinetics of Integrated Methane Recovery and CO 2 Sequestration by Injection of Flue Gas into Permafrost Methane Hydrate Reservoirs. Scientific reports 9, 1-9. doi: https://doi.org/10.1038/s41598-019-52745-x.

Hassanpouryouzband, A., Yang, J., Tohidi, B., Chuvilin, E., Istomin, V., Bukhanov, B., 2019b. Geological CO2 capture and storage with flue gas hydrate formation in frozen and unfrozen sediments: method development, real time-scale kinetic characteristics, efficiency, and clathrate structural transition. ACS Sustainable Chemistry and Engineering 7, 5338-5345. doi: https//:pubs.acs.org/doi/abs/10.1021/acssuschemeng.8b06374.

Hassanpouryouzband, A., Yang, J., Tohidi, B., Chuvilin, E., Istomin, V., Bukhanov, B., Cheremisin, A., 2018a. CO2 capture by injection of flue gas or CO2–N2 mixtures into hydrate reservoirs: Dependence of CO2 capture efficiency on gas hydrate reservoir conditions. Environmental science and technology 52, 4324-4330. doi: https://pubs.acs.org/doi/abs/10.1021/acs.est.7b05784.

Hassanpouryouzband, A., Yang, J., Tohidi, B., Chuvilin, E., Istomin, V., Bukhanov, B., Cheremisin, A., 2018b. Insights into CO2 capture by flue gas hydrate formation: gas composition evolution in systems containing gas hydrates and gas mixtures at stable pressures. ACS Sustainable Chemistry and Engineering 6, 5732-5736. doi: https//:pubs.acs.org/doi/abs/10.1021/acssuschemeng.8b00409.

Jafari, I., Masihi, M., Zarandi, M.N., 2018. Scaling of counter-current imbibition recovery curves using artificial neural networks. Journal of Geophysics and Engineering 15, 1062-1070. doi: https://doi.org/10.1088/1742-2140/aa9fe3.

Kennedy, J., 1997. The particle swarm: social adaptation of knowledge, Proceedings of 1997 IEEE International Conference on Evolutionary Computation (ICEC'97). IEEE, pp. 303-308. doi :

Kennedy, J., Eberhart, R., 1995. Particle swarm optimization, Proceedings of ICNN'95-International Conference on Neural Networks. IEEE, pp. 1942-1948. doi :

Keshavarzi, R., Jahanbakhshi, R., 2013. Real-time prediction of pore pressure gradient through an artificial intelligence approach: a case study from one of middle east oil fields. European journal of environmental and civil engineering 17, 675-686. doi: https://doi.org/10.1080/19648189.2013.811614.

Kisi, O., Parmar, K.S., 2016. Application of least square support vector machine and multivariate adaptive regression spline models in long term prediction of river water pollution. Journal of Hydrology 534, 104-112. doi: https://doi.org/10.1016/j.jhydrol.2015.12.014.

Lima, C.A., Coelho, A.L., Eisencraft, M., 2010. Tackling EEG signal classification with least squares support vector machines: A sensitivity analysis study. Computers in Biology and Medicine 40, 705-714. doi: https://doi.org/10.1016/j.compbiomed.2010.06.005.

Liu, H., 2017. Principles and applications of well logging. Springer.

Mustafa, M., Rezaur, R., Rahardjo, H., Isa, M., 2012. Prediction of pore-water pressure using radial basis function neural network. Engineering Geology 135, 40-47. doi: https://doi.org/10.1016/j.enggeo.2012.02.008.

Osborne, M.J., Swarbrick, R.E., 1997. Mechanisms for generating overpressure in sedimentary basins: A reevaluation. AAPG bulletin 81, 1023-1041. doi: https://doi.org/10.1306/522B49C9-1727-11D7-8645000102C1865D.

Pedersen, M.E.H., Chipperfield, A.J., 2010. Simplifying particle swarm optimization. Applied Soft Computing 10, 618-628. doi :

Polito, C.P., Green, R.A., Lee, J., 2008. Pore pressure generation models for sands and silty soils subjected to cyclic loading. Journal of Geotechnical and Geoenvironmental Engineering 134, 1490-1500. doi: https://doi.org/10.1061/(ASCE)1090-0241(2008)134:10.(۱۴۹۰)

Rehm, B., Schubert, J., Haghshenas, A., Paknejad, A.S., Hughes, J., 2013. Managed pressure drilling. Elsevier.

Sayers, C.M., Johnson, G.M., Denyer, G., 2002. Predrill pore-pressure prediction using seismic data. Geophysics 67, 1286-1292. doi: https://doi.org/10.1190/1.1500391.

Shi, Y., Wang, C.Y., 1986. Pore pressure generation in sedimentary basins: overloading versus aquathermal. Journal of Geophysical Research: Solid Earth 91, 2153-2162. doi: https://doi.org/10.1029/JB091iB02p02153.

Stephen, J.E., Kumar, S.S., Jayakumar, J., 2014. Nonlinear modeling of a switched reluctance motor using LSSVM-ABC. Acta Polytechnica Hungarica 11, 143-158. doi :

Suykens, J.A., Vandewalle, J., 1999. Least squares support vector machine classifiers. Neural processing letters 9, 293-300. doi: https://link.springer.com/article/10.1023/A:1018628609742.

Tsujinishi, D., Abe, S., 2003. Fuzzy least squares support vector machines for multiclass problems. Neural Networks 16, 785-792 .doi: https://doi.org/10.1016/S0893-6080(03)00110-2.

Vapnik, V., 2013. The nature of statistical learning theory. Springer science & business media.

Yang, X.-S., Papa, J.P., 2016. Bio-inspired computation and applications in image processing. Academic Press.

Yarveicy, H., Moghaddam, A.K., Ghiasi, M.M., 2014. Practical use of statistical learning theory for modeling freezing point depression of electrolyte solutions: LSSVM model. Journal of Natural Gas Science and Engineering 20, 414-421. doi: https://doi.org/10.1016/j.jngse.2014.06.020.

Yeganeh, M., Masihi, M., Fatholahi, S., 2012. The estimation of formation permeability in a carbonate reservoir using an artificial neural network. Petroleum science and technology 30, 1021-1030. doi: https://www.tandfonline.com/doi/abs/10.1080/10916466.2010.490805.

Yoshida, C., Ikeda, S., Eaton, B.A., 1996. An investigative study of recent technologies used for prediction, detection, and evaluation of abnormal formation pressure and fracture pressure in North and South America. OnePetro. doi: https://doi.org/10.2118/36381-MS.

Yu, L., Chen, H., Wang, S., Lai, K.K., 2008. Evolving least squares support vector machines for stock market trend mining. IEEE transactions on evolutionary computation 13, 87-102. doi: https://doi.org/10.1109/TEVC.2008.928176.

Yuan, X., Chen, C., Yuan, Y., Huang, Y., Tan, Q., 2015. Short-term wind power prediction based on LSSVM–GSA model. Energy Conversion and Management 101, 393-401. doi: https://doi.org/10.1016/j.enconman.2015.05.065.

Zhang, J .۲۰۱۱ ,.Pore pressure prediction from well logs: Methods, modifications, and new approaches. Earth-Science Reviews 108, 50-63. doi: https://doi.org/10.1016/j.earscirev.2011.06.001.

Zhang, J., Yin, S., 2017. Real-time pore pressure detection: indicators and improved methods. Geofluids 2017. doi: https://www.hindawi.com/journals/geofluids/2017/3179617./

Zheng, H., Liao, R., Grzybowski, S., Yang, L., 2011. Fault diagnosis of power transformers using multi-class least square support vector machines classifiers with particle swarm optimisation. IET Electric Power Applications 5, 691-696. doi: https://doi.org/10.1049/iet-epa.2010.0298.